Supplement of Earth Surf. Dynam., 12, 301–320, 2024
https://doi.org/10.5194/esurf-12-301-2024-supplement

Earth Surface Dynamics
Open Access
EGU

Supplement of

Flexural isostatic response of continental-scale deltas to climatically driven sea level changes

Sara Polanco et al.

Correspondence to: Sara Polanco (sara.moronpolanco@sydney.edu.au)

PART 1

The repository https://github.com/saraemp/egusphere-2023-53 contains the codes necessary to produce the model set up, the input and boundary conditions and post-processing codes used to produce the simulations presented in this paper.

PART 2

Figures referenced in the paper to explain various aspects of the model.

Constitutive equations

$$\frac{\partial z}{\partial t} = -\nabla \cdot qs + u$$

Change in elevation or bathymetry **z** through time **t**

Sediment flux [m²/yr]

Uplift or subsidence [m/yr]

River incision

Hillslope diffusion

$$-\varepsilon(PA)^m(\nabla Z)^n - \kappa\nabla^2 Z$$

Erodibility [1/yr]

Precipitation [m/yr]

Drainage Area [m²]

Topographic gradient

Diffusivity [m²/yr]

Topographic gradient

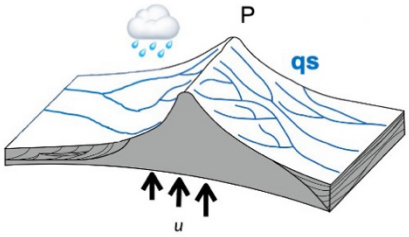

Power function of topographic gradient ∇z and contributing drainage area A

m, n positive dimensionless constants = how incision rate scales with bed shear stress

ε, k are scale-dependent, depend mainly on lithology, precipitation

Flexural deformation

gFlex (Wickert, 2016)

Elastic bending of the lithosphere in response to loading and unloading

Flexural deflection of the Earth's surface

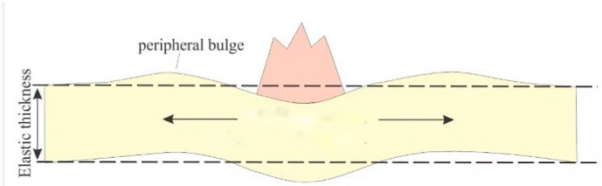

$$D\nabla^2\nabla^2\omega + \Delta\rho g\omega = ql$$

Density contrast between the mantle and the loading material [kg/m³]

Vertical adjustment Elastic plate [m]

Flexural rigidity [Nm]

stress due to loading or unloading [Pa]

Young's modulus [Pa]

Plate effective elastic Thickness [m]

$$D = \frac{ET_e^3}{12(1-\nu^2)}$$

Poisson's ratio

Figure S1. Top: Constitutive equations used in BADLANDS (Salles & Hardiman, 2016) and bottom: Constitutive equations used in gflex (Wickert, 2016). BADLANDS complete documentation and code are available online at https://badlands.readthedocs.io/en/latest/ and https://github.com/badlands-model

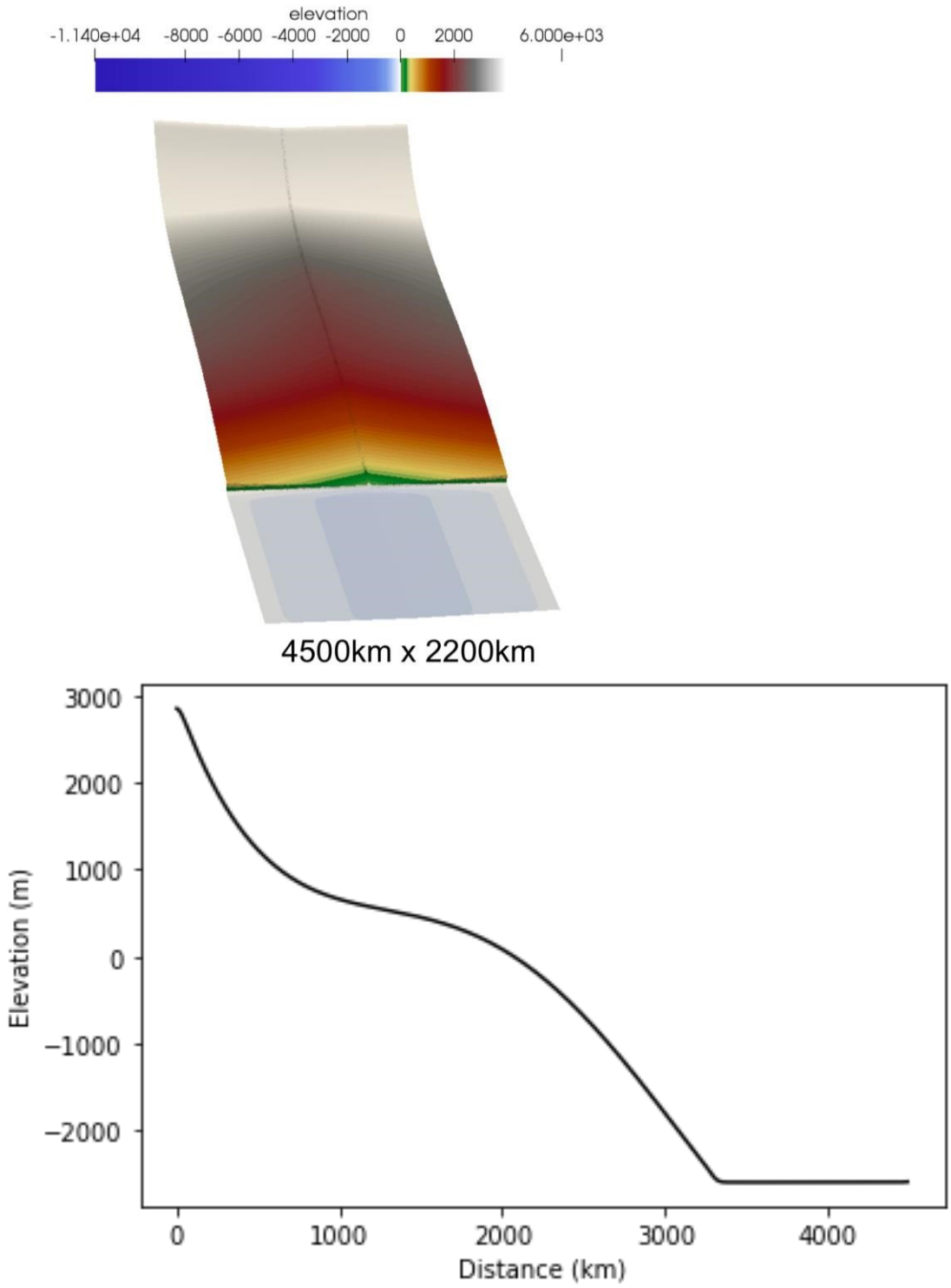

Figure S2. Planview of model setup (top) and cross-section in the middle of the modeling domain. The initial configuration of the modeling domain resembles the topography of a natural source-to-sink system with 3400 m elevation in the headwaters, a length of 4500 km, a downstream-decreasing fluvial channel slope, and successive inflections in gradient associated with the coastal-plain to continental shelf and shelf to slope transitions. To ensure that our simulated drainage basin produces a point-source for sediment input to the marine domain we imposed a longitudinal topographic low in the middle of the model.

Sensitivity tests

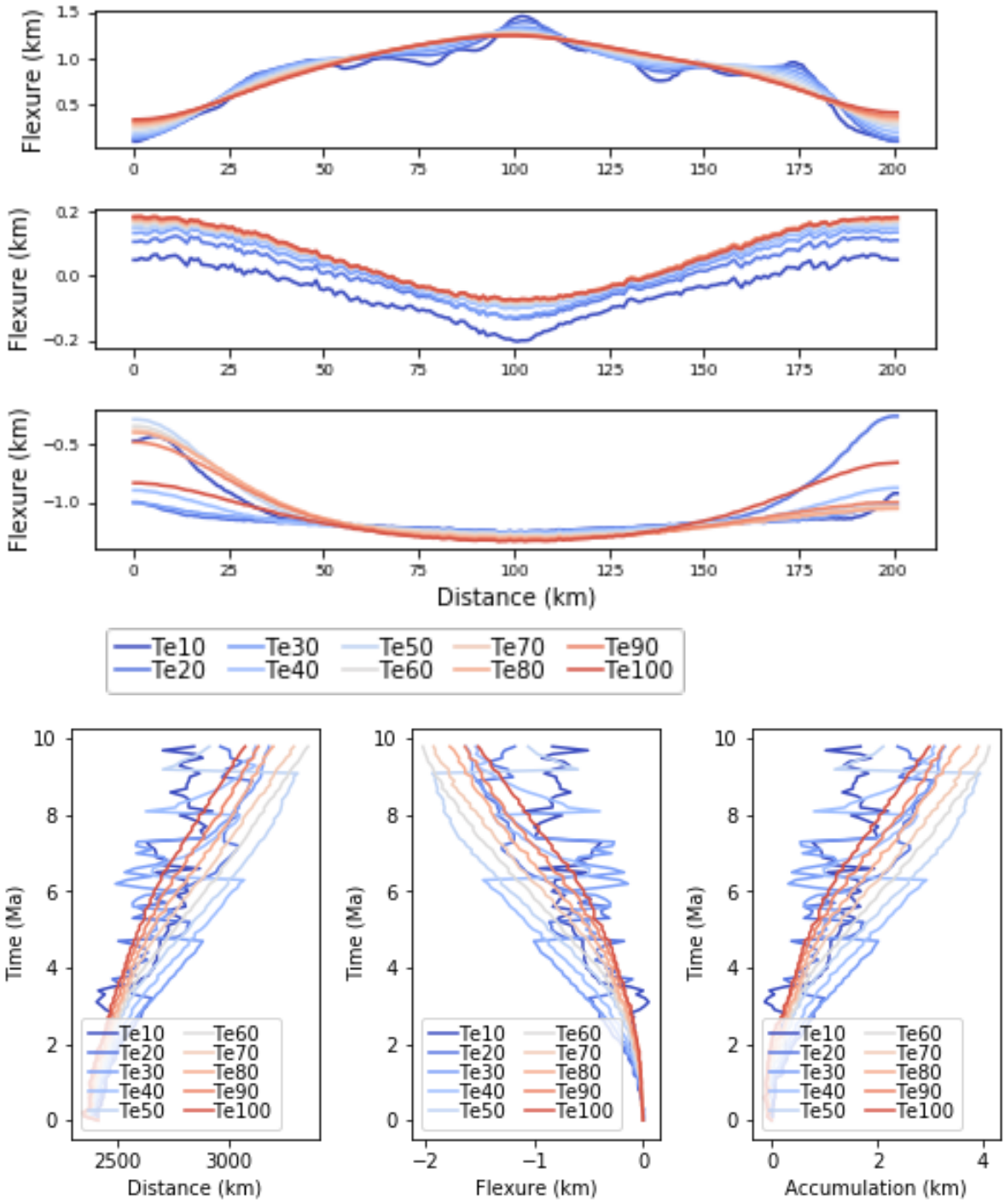

Figure S3. Results of the sensitivity tests with different effective elastic thickness values (top) along three cross sections at arbitrary locations in the river mouth and (bottom) travel distance, flexure and accumulation at the river mouth.

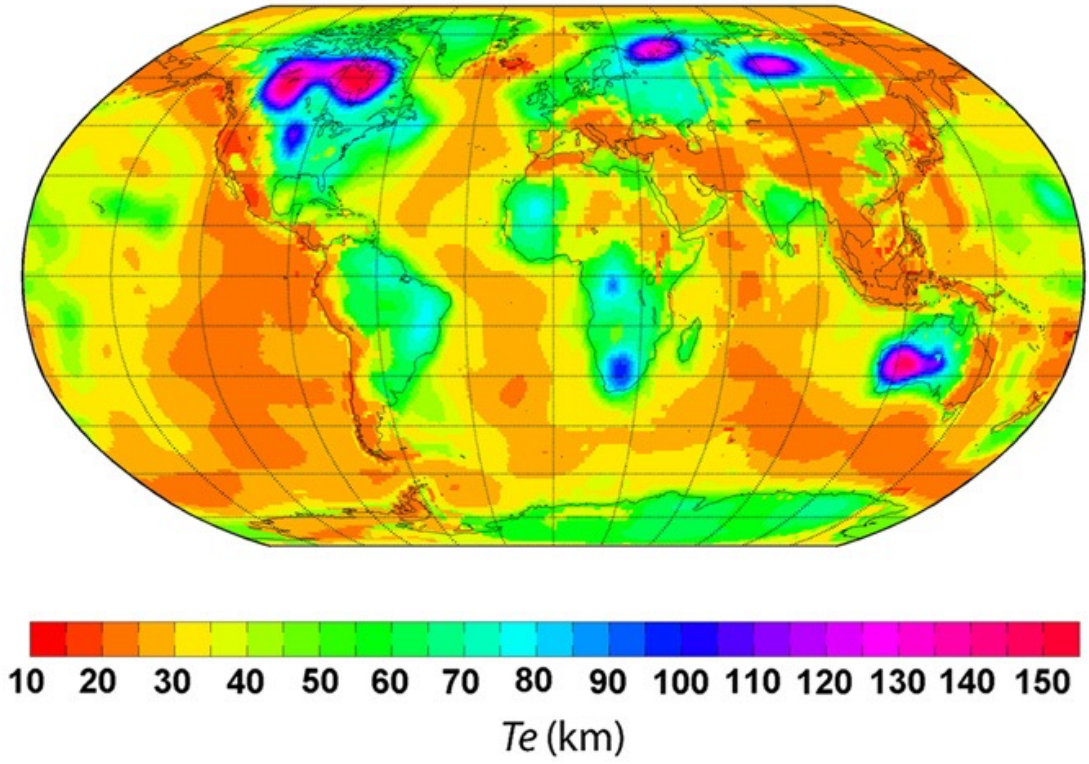

Figure S4. Effective elastic thickness (Te) of the lithosphere (km). For flexurally-compensated models, we use an effective elastic thickness (Te) of 50 km. This value is within the range observed in passive margins. Modified from Tesauro et al., (2012).

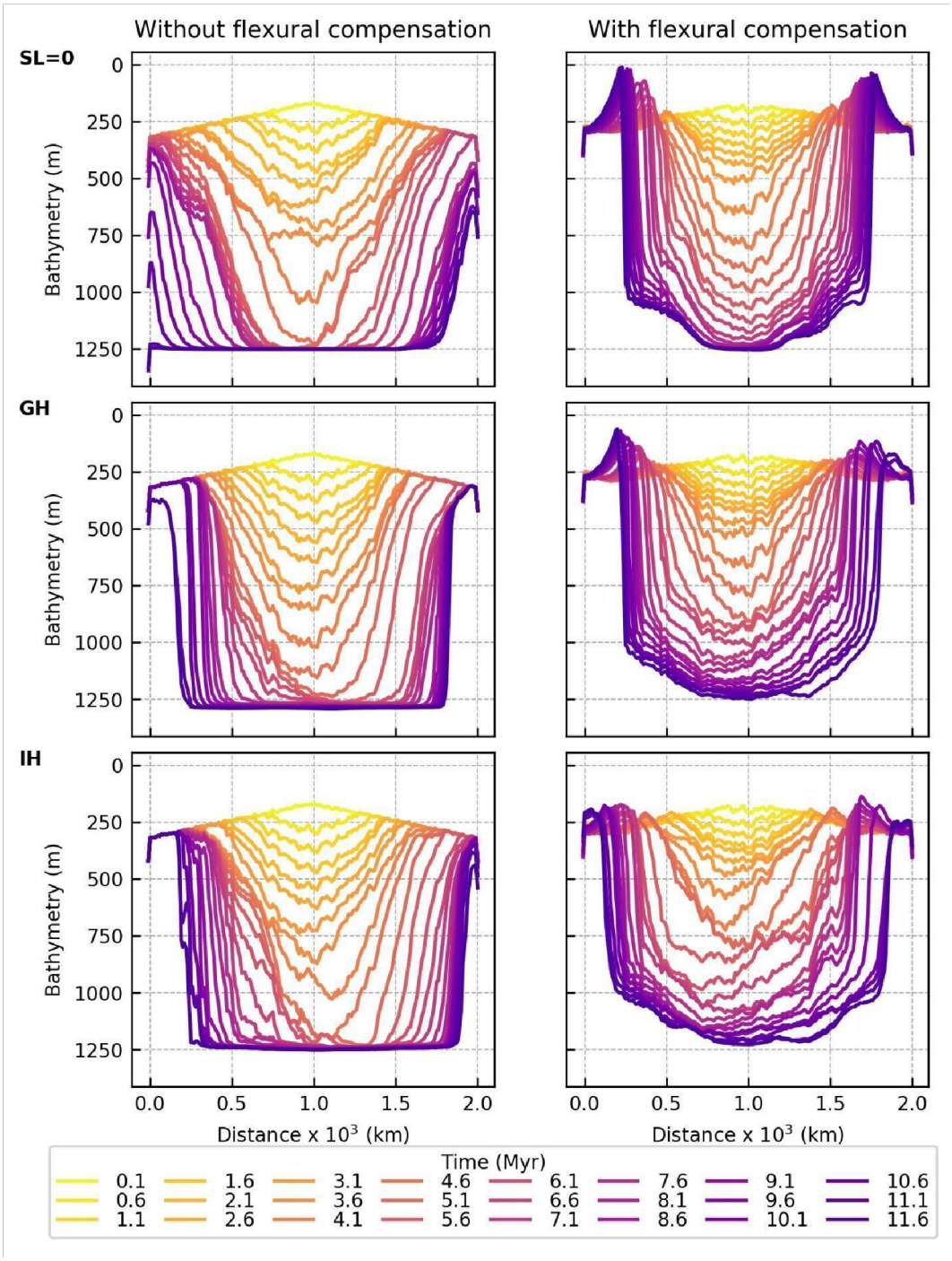

Figure S5 Along strike cross-sections showing the comparison of the bathymetric evolution for simulations without (first column) and with (second column) flexural compensation for different sea-level scenarios. SL=0 constant sea-level, GH= greenhouse, IH= icehouse. The bulges on each of the sides of the deltaic depocenters are the result of the uplift generated by the flexural compensation while the curvature on the bottom of the depocenter is caused by the flexural deflection. Note how both the bulges and curvatures are absent in the simulations without flexural compensation.

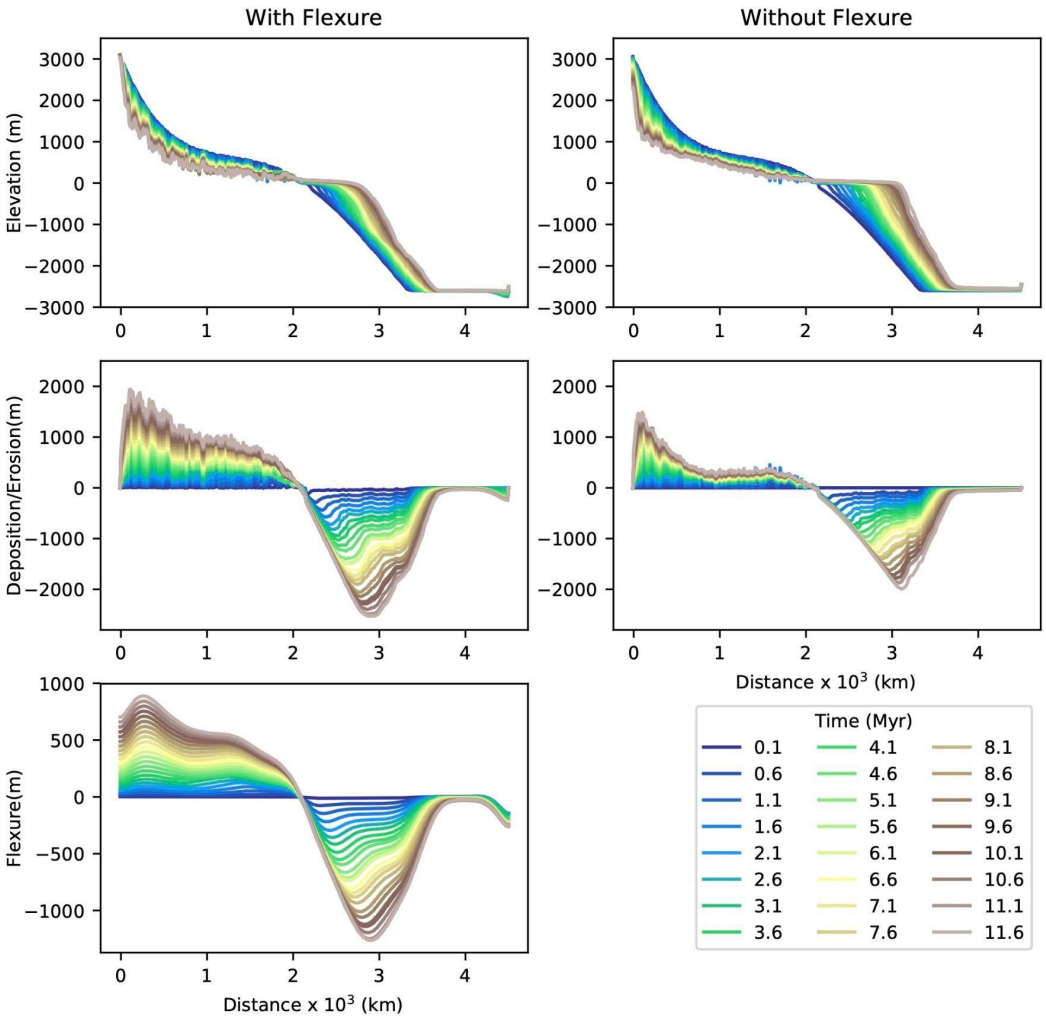

Figure S6. Down-dip shelf-to-slope profile showing the comparison of the temporal evolution of the elevation|bathymetry, deposition|erosion and flexural deflection, for simulations without (first column) and with (second column) flexural compensation. The peripheral bulges landward and alongshore of the deltaic depocenters are the result of the uplift and subsidence are generated by the flexural compensation.

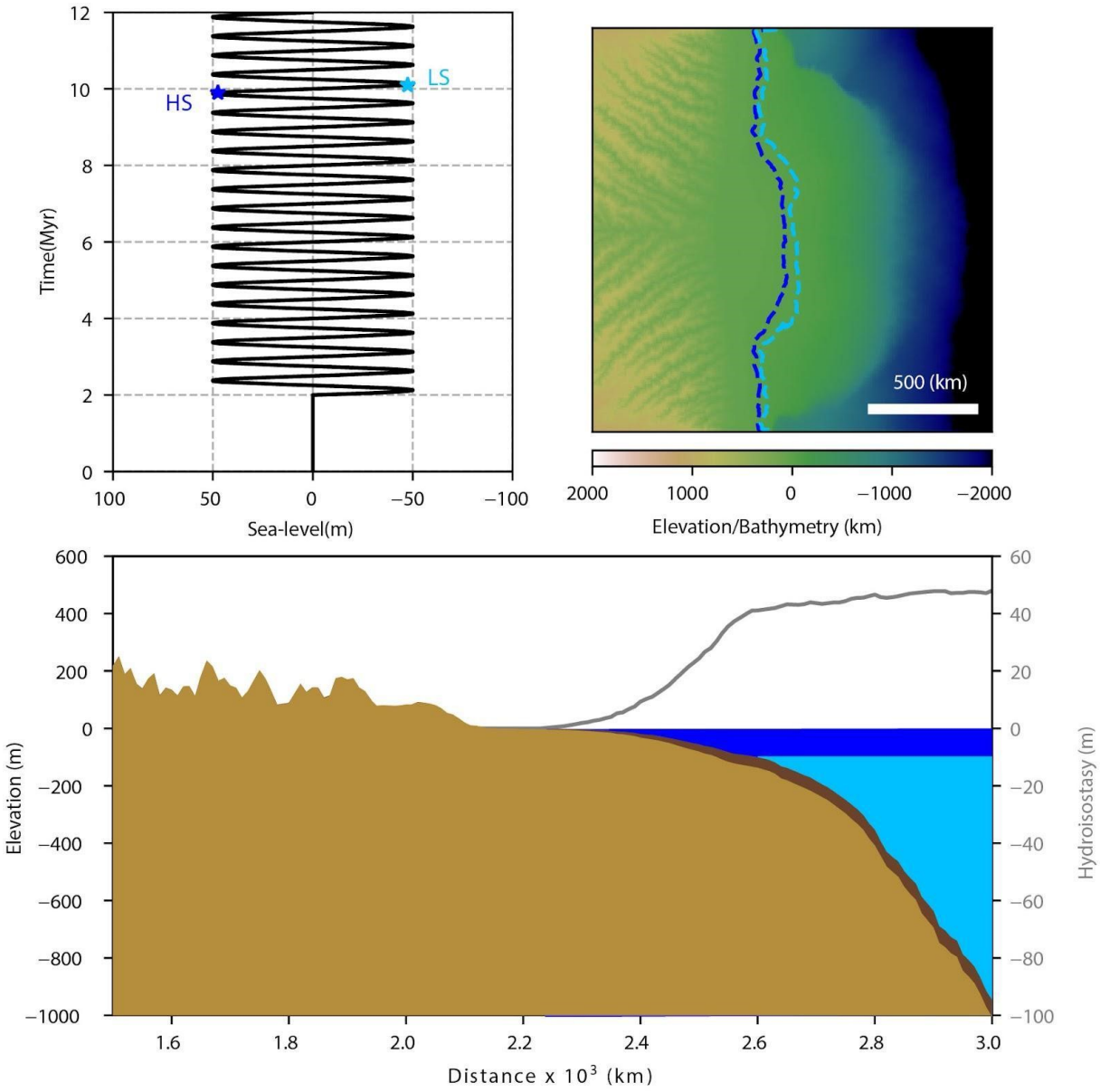

Figure S7. Model results showing the uplift generated by the hydro-isostatic adjustment associated with a sea-level fall of 100 m and exposure of the shelf. Upper left: Synthetic sea-level curve with an amplitude of 50 m and a frequency of 500 Kyr, the asterisks show the particular time step of the simulation where the results were extracted. HS = highstand (dark blue) LS = lowstand (light blue). Upper right: output of numerical simulations showing elevation, bathymetry and shoreline position at HS (dark blue) and LS (light blue). Bottom: Longitudinal profile for HS (dark blue) and LS (light blue). Horizontal lines show the position of the sea-level. The vertical difference in bathymetry between the HS and LS can be explained by the uplift created by the hydroisostasy (dashed gray line) related to the change in sea level between HS and LS. Model output elevation was adjusted to correspond to sea-level (or zero).

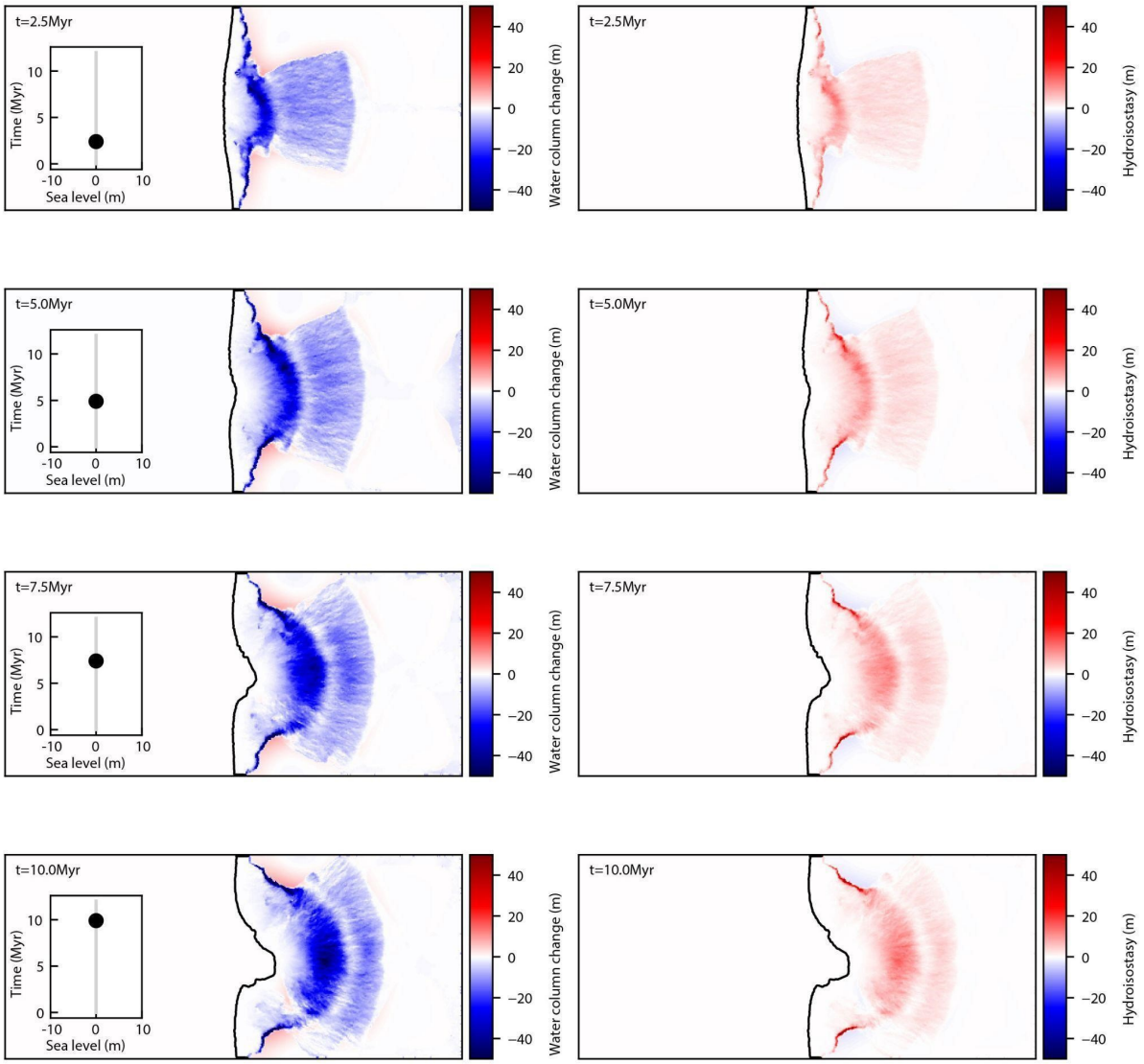

Figure S8. Map views showing the temporal evolution of the change in water column (left) and associated hydro-isostasy (right) in the numerical simulations with no sea-level change. Insets on the left panels show the imposed sea-level curve and the round symbol the point in time when the simulation output was taken. Because sea level is constant changes in relative sea level and hydro-isostasy are associated with the progradation of the sediment wedge which in turn causes variations in the gradient of the shelf edge' slope but not around the shoreline. Note how the hydro-isostasy is consistently positive through time.

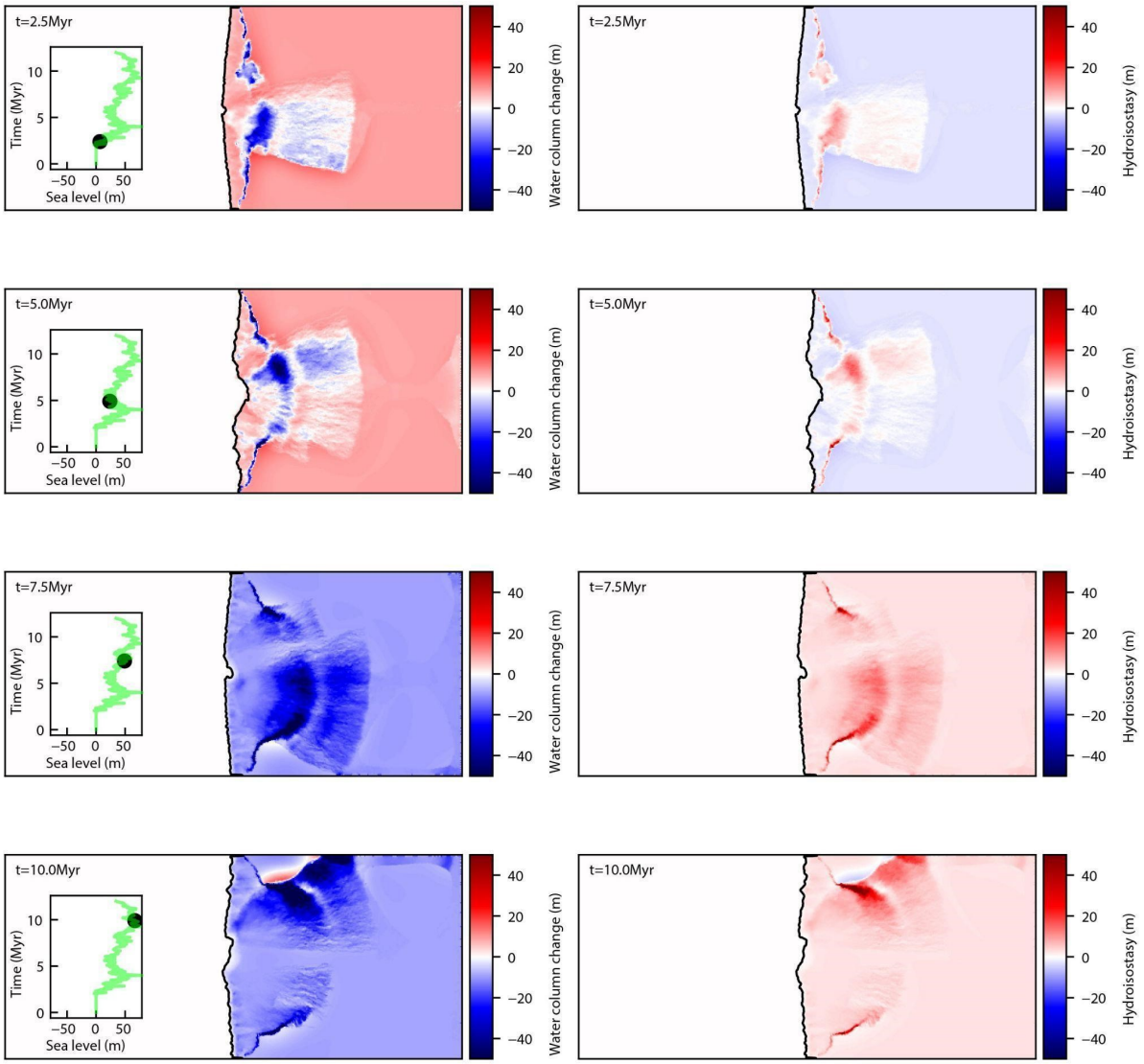

Figure S9. Map views showing the temporal evolution of the change in water column (left) and associated hydro-isostasy (right) in the numerical simulations with a green-house sea-level curve. Insets on the left panels show the imposed sea-level curve and the round symbol shows the point in time when the simulation output was taken. The spatial variation of the hydro-isostasy is a function of elevation changes as the sediment wedge progrades and fluctuations in sea level. Note the changes in the direction of hydro-isostasy through time, which contrasts with the results from the simulations with no sea-level change presented in the previous figure.

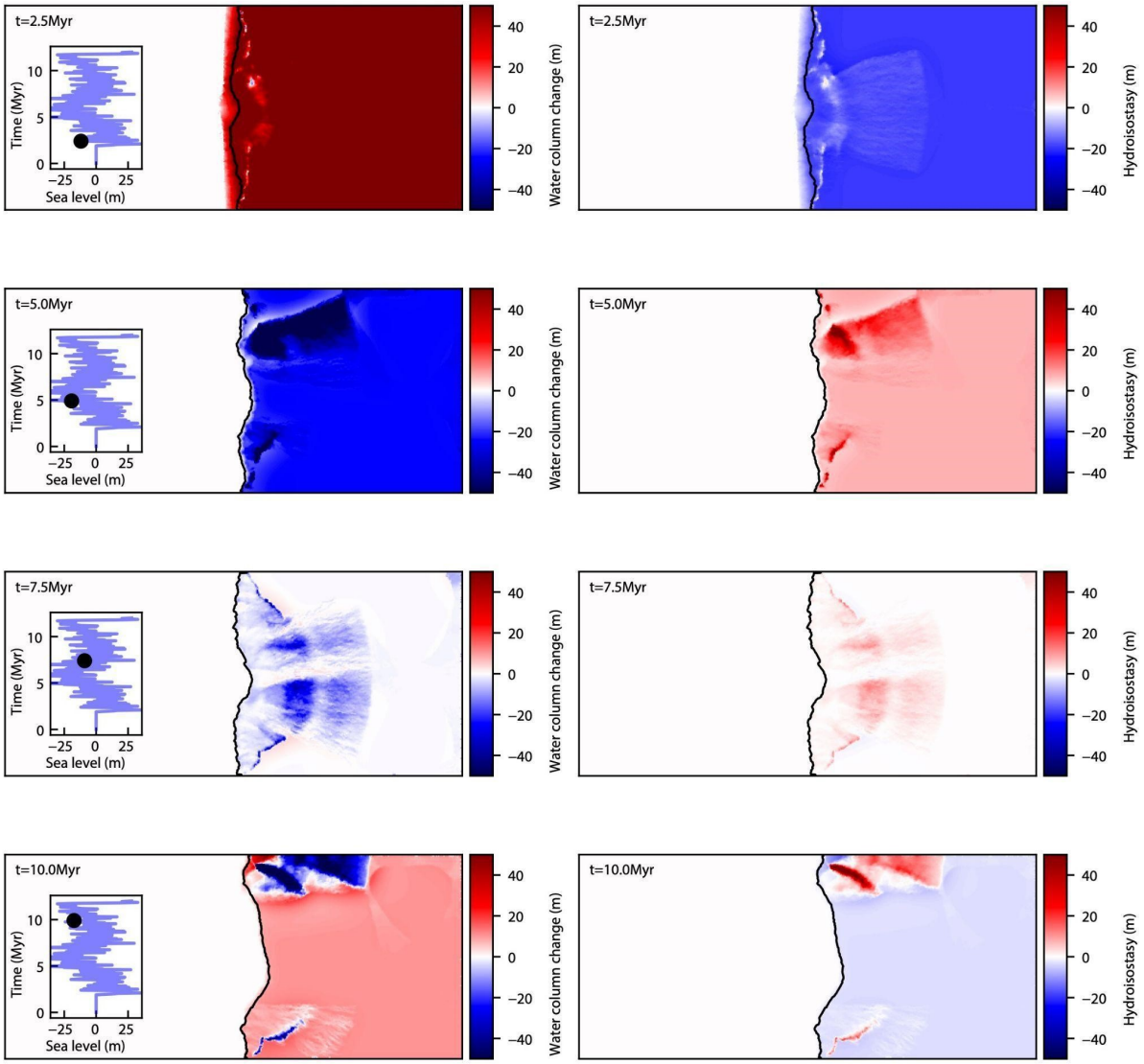

Figure S10. Map views showing the temporal evolution of the change in water column (left) and associated hydro-isostasy (right) in the numerical simulations with an ice-house sea level curve. Insets on the left panels show the imposed sea-level curve and the round symbol shows the point in time when the simulation output was taken. The spatial variation of the hydro-isostasy is a function of elevation changes as the sediment wedge progrades, the valley incision during sea-level fall and fluctuations in sea level. Changes in the direction of hydro-isostasy through time are more dramatic than on the numerical simulations with a green-house sea level curve.

Table S1 Mean values for river mouth length and mean maximum accumulation values measured at each time step of the simulation. The statistics presented here are from 2Myr to 12Myr, which is when we imposed different sea-level fluctuations to simulations.

	Mean river mouth length (km) Non-Flexural simulations	Mean river mouth length (km) Flexural simulations	p-value	Mean maximum accumulation (m) Non-Flexural simulations	Mean maximum accumulation (m) Flexural simulations	p-value
SL=0	2538	2425	5.44E-05	961	1724	8.43E-09
f500Kyr A25m	2491	2340	3.64E-07	1188	1392	5.19E-02
f5Myr A25m	2523	2354	7.14E-07	1215	1702	2.22E-04
GH	2310	2250	2.00E-03	1067	1394	1.44E-03
IH	2561	2341	1.07E-11	1052	1415	4.16E-04